Published in: *Network*, 6:271-288, 1995.

Low Spiking Rates in a Population of Mutually Exciting Pyramidal Cells

Short title: Low Rates in a Population of Pyramidal Cells

Erik Fransén and Anders Lansner*

SANS – Studies of Artificial Neural Systems
Dept. of Numerical Analysis and Computing Science
Royal Institute of Technology, S–100 44 Stockholm, Sweden

*To whom correspondence should be addressed
Email: ala@sans.kth.se

January 26, 1995

Abstract

In a recurrent artificial neural network, the units active in an attractor state typically reach their maximum activity value while the others are quiescent. In contrast, recordings of cortical cell activity *in vivo* rarely reveal cells firing at their maximum rate. This discrepancy has been one of the main arguments against using attractor networks as models of cortical associative memory.

In this study we show that low rate sustained after-activity can be obtained in a simulated network of mutually exciting pyramidal cells. This is achieved by assuming that the synapses in the network are of a saturating type. When the application of a monoamine neuromodulator is simulated, after-activity with firing rates around 60 s^{-1} can be produced. The firing pattern of the network was found to be similar to that of the experimentally most comparable system, the disinhibited hippocampal slice. The results obtained are robust against simulated biological variation and background noise.

1 Introduction

In his 1949 book "The Organization of Behavior", Hebb put forward the cell assembly - a group of cells connected by mutual excitatory synapses - as the basic entity for mental representation (Hebb 1949). It was assumed to be formed by coactivation of cells together with the action of Hebbian synapses. Its existence was manifested in different associative memory and Gestalt perception phenomena, like pattern completion and perceptual rivalry. Later the cell assembly theory has been extended in different ways, *e.g.* by including lateral inhibition between assemblies as a means to prevent spread of activity from one active assembly to overlapping ones (Milner 1957).

A recurrent attractor artificial neural network (ANN) of the Hopfield type (Hopfield 1982) can be regarded as a mathematical formulation of the cell assembly theory. In order to assess the biological relevance of such network models, we have previously investigated the function of an attractor network composed of realistically modeled cells (Lansner and Fransén 1992). It was shown that such a network readily displays attractor after-activity as well as pattern reconstruction and rivalry effects.

In an attractor network the units active in a certain fix point state attain their maximum activity level whereas all other units are quiescent. This is due to the pronounced feedback excitation of the recurrent network structure. Given that the activity levels of the ANN units are analogous to instantaneous firing rates of nerve cells, this pattern of activity can be compared to experimental data. Typically, the firing frequency of a cortical pyramidal cell can reach up to some 300 Hz when driven by an injected current (McCormick *et al.* 1985). However, from experimental *in vivo* recordings it is clear that cortical pyramidal cells rarely operate at frequencies higher than 20–60 Hz (Miyashita 1988; Miyashita and Chang 1988; Fuster and Jervey 1982; Funahashi *et al.* 1989, 1990; Abeles *et al.* 1990). This discrepancy, regarding what part of the units' dynamic range is used, has been one of the strongest arguments against attractor network models of cortical associative memory previously put forward, see *e.g.* Amit *et al.* (1990), Lansner and Fransén (1992) and Hasselmo *et al.* (1992).

Several authors have addressed this problem and proposed mechanisms for obtaining low activ-

ity levels in attractor ANNs. Examples of mechanisms suggested are fast inhibitory feed-back (Amit and Treves 1989; Buhmann 1989; Rubin and Sompolinsky 1989) and noise driven activity with sub-threshold excitation (Amit *et al.* 1990; Amit and Tsodyks 1991a, 1991b). A low average activity resulting from having only a few highly active cells (sparse activity) in a large population is not compatible with experimental recordings. See also Amit and Tsodyks (1991a) and Peretto (1992) for a discussion.

The work presented here complements earlier studies by introducing another mechanism that gives low firing rates in an attractor network with biologically detailed cell models as units. We show that by introducing strongly saturating synapses in a network of pyramidal cells, such activity can be robustly produced. In addition, this is most likely a better model of the synapses connecting cortical pyramidal cells (Andersen 1986) than one assuming summing synaptic conductances. For a recurrent network of cells with summing synapses, the frequency limiting factors are related to the spike generating mechanisms of the receiving cell, *i.e.* the action potential width, mainly the sodium and potassium dynamics, together with the cell membrane time constant. With saturating synapses as those proposed here, the dominating frequency limiting factors are instead the synaptic maximum conductances and the time constants for closing of synaptic ion channels. The simulation results presented in the following also illustrate the fact that a simple network of biologically realistic units is capable of a much richer dynamics than its corresponding ANN.

2 Network Structure and Cell Model

In this study we have used the general purpose simulator, SWIM, intended for numerical simulation of networks of biologically realistic model neurons (Ekeberg *et al.* 1994, 1991). The model neurons may be composed of an arbitrary number of iso-potential compartments. Voltage dependent ion channels for Na, K, Ca, and Ca-dependent K are modeled using Hodgkin-Huxley-like equations. Synaptic interaction between model neurons may include both conventional kainate/α-amino-3-hydroxy-5-methyl-4-isoxazolepropionic acid (AMPA) synapses and N-methyl-D-aspartate (NMDA) receptor gated synapses. The cells used in the simulations described here are of intermediate

complexity. Details of the mathematical model used in SWIM is found in (Ekeberg *et al.* 1991; Wallén *et al.* 1992; Tråvén *et al.* 1993). The parameter values used here are given in the Appendix.

Below we describe important aspects of the structure of the simulated network and the properties of the model cells and synapses.

2.1 Structure of the network simulated

The full attractor network model, described in Lansner and Fransén (1992), is composed of pyramidal cells and fast spiking local inhibitory interneurons. When a set of patterns are memorized using a correlation based learning rule the pyramidal cells in the same cell assembly, corresponding to one of the patterns, are connected by means of strengthened excitatory synapses, whereas pyramidal cells that never appear in the same pattern instead inhibit each other via local inhibitory interneurons. When a memorized pattern is active, *i.e.* the network is in the corresponding attractor state, the active pyramidal cells in an assembly are mutually exciting each other and at the same time they keep other cells silent by means of lateral inhibition.

In the present study, our aim has been to look in detail at the cell activity levels in the attractor state described above. One assembly has been "cut out" of the full network model, and the network thus only consists of excitatory cells. In this way the intrinsic dynamics guiding the activity of this group of cells and the mechanisms controlling spiking rates could be studied. The biological system closest to our network that has been studied experimentally and by means of simulations is the disinhibited hippocampal slice. In sect 3.5 we make a comparison with results by Traub *et al.* (1992).

The "cut out" cell population simulated here consists of 50 mutually interconnected pyramidal cells of the regularly spiking (RS) type (see sect 2.2 for details of the cell model). The soma diameters are sampled from a normal distribution with a mean of 21 μm and a standard deviation of 5 %. The relatively small spread introduced here has a large enough effect on excitability to prevent artifacts that might otherwise appear in a population of simulated identical cells. The actual biological variation in cell diameters is larger, but data regarding the variation in electrical properties (which is what really determines the behavior) is incomplete and not accounted for here.

This small network is fully connected but connectivity is diluted for larger sizes (see sect 3.4). If nothing else is stated the following applies: the kainate/AMPA and NMDA components of a synapse have a maximum conductance of 80 and 560 pS respectively and a standard deviation of 20 %. The summed axonal conduction and synaptic time delays have a mean of 2 ms and a standard deviation of 2.5 %. Typical examples of EPSPs, produced by the different types of synapses, following a single activation are: the kainate/AMPA component has amplitude 0.10 mV and latency to peak 15.7 ms, the NMDA component has amplitude 0.07 mV and latency to peak 35.4 ms and the combined kainate/AMPA and NMDA EPSP has amplitude 0.13 mV and latency to peak 24.5 ms.

The simulations were made on a DECsystem 5000/200 UNIX workstation. A time step of 50 μs was used and a simulation of 1 s activity took about 20 minutes of computing time. In all network simulations the system was run for 1 s simulated time before the experiment started (to reach "steady state" conditions). To avoid common-input synchronization artifacts, current stimulation start and stop times were generated, for each cell, from a normal distribution with a standard deviation of 5 ms. All current strengths were generated with a standard deviation of 10 %. Cell firing rates calculated from interspike intervals are here given in s^{-1}, as opposed to repetitive firings given in Hz. In the mean spike-rate plot the inverse interspike intervals are averaged over all cells in 10 ms bins.

2.2 The neocortical pyramidal cell model

The cell model, RS, is intended to simulate a neocortical pyramidal cell of the regularly spiking type (McCormick *et al.* 1985). It could represent *e.g.* a cell of lamina II/III. For the soma we included Na, K, Ca and Ca-dependent K channels. Tightly connected to the soma compartment is a small initial segment compartment which has only Na and K channels. Three dendritic compartments are used to model the apical dendrite and one is used for the basal dendrite. All dendritic compartments are of equal area (4 times the soma) and electrotonic length. Except for synaptic ion channels, the model pyramidal cell dendrites are purely passive.

The late afterhyperpolarization (AHP) plays a key role in controlling the excitability of the

cell and hence its repetitive firing characteristics (Gustafsson and Wigström 1981). Here the late AHP is modeled by three parameters (Ekeberg *et al.* 1991; Brodin *et al.* 1991): Ca-pool inflow rate, Ca-pool decay time and Ca-dependent K channel density (total conductance). To find appropriate values for these, given the variation in experimental data, several sources were used. Our primary source of data was the diagrams in McCormick *et al.* (1985) fig 1D, Stafstrom *et al.* (1984) fig 2A, and Mason and Larkman (1990) fig 10A, displaying spike firing adaptation for several different currents. We also used single traces in McCormick *et al.* (1985), fig 1a,b, Connors *et al.* (1982) fig 5, Stern *et al.* (1992) fig 3b,d, Bernander *et al.* (1992) fig 6, 7, and Mason and Larkman (1990) fig 4 A2, 7 A1. These show the rise time, decay time and depth of the AHP and also adapting spike trains for a particular number of spikes (currents) and resting potentials. The difference in adaptation between *in vitro* and *in vivo* registrations is discussed by Bernander *et al.* (1992). A ratio of 10–20 % between first and steady-state inter-spike interval time for *in vitro* measurements and 40 % for *in vivo* was reported. Since data from *in vitro* experiments were used to set the conductance of the Ca-dependent K channels, the value was multiplied by a factor 0.49 to reflect the above mentioned *in vivo* conditions.

The conductance of the Ca-dependent K channel may be affected by several monoamine neuromodulators such as serotonin, noradrenaline and histamine as well as by acetylcholine and CRF (corticotropin-releasing factor) (Nicoll *et al.* 1990) [1], thereby changing the adaptation properties of the cell (Colino and Halliwell 1987; McCormick 1989; Madison and Nicoll 1982). To model the influence of the modulator, the conductance through the Ca-dependent K channels was multiplied by a factor (KCa) in the range 0 to 1. Sample spike trains and spike adaptation curves for our RS-cell are given in fig. 1 and 2 respectively.

(Figure 1 and 2 somewhere here)

2.3 The model synapse

The basic model synapse of SWIM has six parameters, as described in Ekeberg *et al.* (1994) and Tråvén *et al.* (1993), *i.e.* an axonal conduction and synaptic delay, a time constant for opening,

[1] We will use the term "modulator" for a neuromodulator having this effect on the Ca-dependent K channel.

a time during which the synapse stays open before it starts closing, a time constant for closing, a reversal potential, and a maximum conductance. The NMDA synapse has additionally equations describing the magnesium block (giving its voltage dependence) and calcium pool dynamics. The excitatory RS-RS glutamate synapse used here is of a mixed kainate/AMPA and NMDA type with equally large peak amplitude postsynaptic potentials (PSP) for each type alone. The closing time constants for the different components are 10 ms and 150 ms respectively. The synapse is placed on the medial apical compartment of the receiving cell. It has been estimated (Andersen 1990; Gilbert *et al.* 1990) that the most likely number of synapses from one pyramidal cell to another is one and we assume this is the case in the network simulated here. Calcium entering through the NMDA channels of synapses on the dendrite is assumed to be local and therefore does not affect the somatic Ca-dependent K channels (Müller and Connor 1991; Guthrie *et al.* 1991). For a complete set of synaptic parameter values see the Appendix.

The extent to which a synaptic conductance is accumulating over successive spikes mainly depends on to what degree a released vesicle saturates the postsynaptic receptor pool. For the saturating synapse type we have assumed that full saturation is reached by each presynaptic spike, (see Andersen (1986) and the discussion on summation therein). The synapse is saturating in the sense that the conductance during repetitive firing can only sum up to the peak conductance resulting from a single presynaptic spike. Synapses with a maximum conductance (saturation cut-off) have been used by *e.g.* Traub *et al.* (1992) and (Destexhe *et al.* 1994). For the summing synapse every spike adds a constant amount to the present conductance value. Irrespective of the type of synapse used, the passive membrane will, of course, still temporally sum incoming PSP:s. The difference in driving capability between the summing and the saturating synapse is strongly frequency dependent as seen in fig. 3.

(Figure 3 and 4 somewhere here)

3 Simulation Results

In our earlier investigations we compared the operation of a Hebbian cell assembly network (with several memorized patterns stored) to that of a recurrent ANN (Lansner and Fransén 1992). It was concluded that a simple recurrent network of real neurons would be capable of operating in much the same way as an ANN. When the latter would converge to an attractor state, the former produced after-activity for some 350 ms. Further, the time to reconstruct a pattern, even in the case of ambiguous input, was found to be around 100 ms. This is compatible with experimentally determined perceptual processing times (Thorpe and Imbert 1989). In the following, we study the dynamics of a population of mutually exciting pyramidal cells that, in effect, corresponds to an isolated cell assembly from the previously simulated network.

3.1 Experiments with summing and saturating synaptic drive

In a network like this, an equilibrium situation is at hand when the firing frequency of the cells, f_{out}, equals the firing frequency on every input, f_{in}, required to drive the cells to produce this output. Our neocortical pyramidal cell gives a "log shaped" input-output relation, which in fig. 4 intersects the equilibrium line $f_{in} = f_{out}$ once (the details of fig 4 will be discussed below). The intersection point is stable since a cell, for increased driving frequency, will produce a lower frequency than its driving source, and for decreased driving frequency, will produce higher frequency, bringing the frequency back to the initial value if slightly perturbed. This is where stationary fix point activity, in the absence of any external input, may occur. With different parameter values there may be a second lower intersection point which will then be unstable.

To study the network with different synaptic properties, we carried out a simulation in which an isolated postsynaptic cell was driven by a number of noisy synaptic inputs (Poisson). To have noise rather than a pure frequency reduces synchronization effects (Tråvén *et al.* 1993; Ekeberg 1993). The frequency of the driven cell was then plotted against the source frequency, see fig. 4. This setup allows us to determine the shape of the $f_{in} - f_{out}$ curve and the points of intersection with the $f_{in} = f_{out}$ line. With summing synapses the stable intersection point will be at a frequency

value of some 110 Hz. With saturating synapses the point may be significantly lower, about 70 Hz, the precise value being dependent on the closing time constant, see fig. 4.

The conductance of the synapse also affects the frequency, but the intersection point can not be much lower before the whole curve falls below the $f_{in} = f_{out}$ line and thereafter has no stable point. The saturating synapse potentially has less conductance than the summing one, but this does not give rise to the low frequency stability; it merely affects the scaling factor used to set the maximum conductance (all conductances were tuned to give a starting point at 30 Hz). The modulator level also affects firing frequency, but as fig. 4 was derived for the normal case with pronounced adaptation (no modulator, KCa=1), simulated modulator application can only bring frequency up[2]. Note that summing synapses give a high frequency despite this pronounced adaptation. Further support that neither low synaptic strengths nor adaptation or modulator application give a low rate in the active network will be given in sect. 3.3.

3.2 Saturating synapses in the recurrent network

We now turn to our recurrent network composed of 50 RS-cells connected by saturating excitatory synapses. If a current stimulation is given to all cells, an activity burst is produced. If the stimulation continues a train of bursts will appear with a burst frequency of about 2 Hz, see first second of fig. 5a and 5b. Burst termination is due to an accumulating AHP which produces a delayed reduction of the excitability of the active cells. When the frequency decreases the cells recover and a new burst appears. The frequency of the bursts decreases with an increasing AHP decay time constant and increases with increasing stimulating current strength. If a sufficient number of cells (8–10 cells in fig. 5 and 6) are stimulated by a 50 ms current pulse the entire network will get active in the subsequent burst. This demonstrates that there is some capability for pattern completion. Further, this is a threshold phenomenon, since just a few stimulated cells will not produce any secondary activity (Lansner and Fransén 1994).

[2]This can be seen in fig. 6a and will be further discussed in sect. 3.3

3.3 Effects of neuromodulator application, low rate activity

The dynamics of a network like the one studied here is dramatically affected when application of a neuromodulator changes the cells from adapting to less adapting. For instance, in the previously studied Hebbian cell assembly network (Fransén *et al.* 1993), the mode of operation could be changed from being purely stimulus driven to one of sustained after-activity (intrinsic reverberation). Other examples of modulator simulations are: Introduction of acetylcholine modulation in simulations of the piriform cortex (Liljenström and Hasselmo 1993), making the oscillation frequency change from gamma to theta frequency and the number of oscillations following stimulation to increase; Simulations by Traub *et al.* (1992) of the effect of carbachol to investigate the mechanism behind the low frequency (5 Hz) bursting seen in the hippocampal CA3 *in vitro* preparation (see also sect. 3.5).

If modulator application to our network of active RS-cells is simulated, an initial activity burst is often followed by low rate after-activity, see last second of fig. 5a and 5b. The width and height of the burst immediately following modulator application depends on the precise amount of modulator (and also cell excitability, closed loop time and rate of AHP buildup). A constant current stimulation will raise the level of the plateau somewhat, see center of fig. 5 a. Of more importance, the frequency of the after-activity will be affected by the modulator level (and also the spatial and the temporal summation characteristics of the cell), see fig. 6a. Here the activity of the network is seen for modulator applications ranging from none (KCa=1), to full (KCA=0). As can be seen the frequency increases with modulator application level, as was noted in fig. 4. To see the stability of the after-activity, the "standard" case (KCa=0.6) is displayed for a longer simulation time in fig. 6b. There was no frustration (no cells with only background activity), and the standard deviation of the firing frequencies was 21 Hz. As a comparison two cases with summing synapses are also shown. The two extremes of modulator values were selected to show the full range of rates and adaptations. For both cases the synaptic conductances were tuned to their smallest possible values that still allowed after-activity to persist. The rates are in good agreement with fig. 4. Together with the results of fig. 4 these simulations clearly demonstrate that the frequency of the

driven cell is mainly dependent on the summation properties of the driving synapses.

(Figure 5a and 5b somewhere here)

(Figure 6a and 6b somewhere here)

It is the accumulating, (activity dependent) delayed AHP that produces a negative feedback that affects network dynamics. In some cases it gives oscillations in the mean firing frequency, as in fig. 5a and 6b, and it also affects the threshold where after-activity will appear. Below a certain modulator value no after-activity is produced. The oscillating frequency was typically around 7 Hz (2–10 Hz when the driving current or the calcium dynamics was varied), see fig. 6b. In delayed-response match to sample experiments oscillation frequencies around 5–6 Hz has been reported (Nakamura *etal.* 1991).

3.4 Network size and diluted connectivity

In order to investigate the influence of increased cell numbers and dilution of connectivity, some additional simulations were performed. With larger fully connected networks, after-activity firing rates could be further decreased. For instance, with 200 cells in the network the stable low-limit was 55 s^{-1}. In larger networks a strong dilution of the connectivity was also possible provided that the remaining synapses were strengthened to compensate for the lower number of synapses on each cell. A 100 cell network with the same number of synapses as in our 50 cell network, *i.e.* with 75 % of the potential number of connections removed and the remaining ones strengthened by a factor of 2.5, gave reliable after-activity at 75 s^{-1} and above. A 200 cell network, with 94 % of the connections removed and the remaining ones strengthened by a factor of 5, gave a lowest firing rate of about 70 s^{-1}. Thus, the scaling behavior seems reasonable, and parameter values used also apply to networks with a diluted connectivity.

3.5 Comparing to experiments and simulations of the hippocampus

As described in sect 2.1 our network corresponds to an isolated assembly in a disinhibited network. The firing pattern, burst frequency and burst amplitude can qualitatively be compared to the

simulation results of (Traub *et al.* 1990, 1992). In their work the activity of interconnected pyramidal cells, previously studied experimentally in the CA3 region of the hippocampus, is simulated by a network composed of 1000 CA3 pyramidal cells connected by some 20,000 AMPA synapses. In the experiment the hippocampal *in vitro* slice preparation is treated with carbachol blocking both $GABA_A$ and $GABA_B$ mediated inhibition. Carbachol also has a modulatory effect on the conductance of the Ca-dependent K channels ($g_{K(Ca)}$). We have compared the activity of our network to that of Traub *et.al* . As in their simulations the cells are given a super-threshold current injection in the medial part of the dendritic tree. The results are quite similar, but differences in the behavior between the model of Traub *et.al* of hippocampus (a part of paleocortex) and our model of neocortex, can also be seen at the cellular as well as the network level.

3.5.1 Changing the synaptic strength and the $g_{K(Ca)}$

For small synaptic strengths the population fires at a low regular rate, as seen in the spike histogram, fig. 7a (c.f. Traub *et.al* fig. 3A). At a higher strength an amplitude modulation in the number of spikes per bin occurs. At still higher strengths bursts appear, with silent periods in between bursts. For large synaptic strengths a continuous, amplitude modulated, high frequency firing results. If the cells are completely uncoupled the bursting feature of the cells of Traub *et.al* is apparent and different from the regular firing of our cells. Both networks produce a constant burst frequency for intermediate synaptic strengths. For large synaptic strengths both networks increase their frequency (now the frequency of the amplitude modulation). Our network gives a frequency of 2–3 Hz as opposed to that of Traub *et.al* showing 2–7 Hz. If our network is connected with only kainate/AMPA synapses, as that of Traub *et.al* , it can burst at this higher frequency. Thereby the similarity in burst shape and amplitude also gets larger. There is a small amplitude for low synaptic strengths, a medium amplitude for continuous high frequency firing and a high amplitude of the bursts.

(Figure 7a and 7b somewhere here)

The effect of varying $g_{K(Ca)}$ is also studied, see fig 7b (c.f. Traub *et.al* fig. 4). Below some specific value of $g_{K(Ca)}$ the cells fire continuously with an amplitude modulation in the number of spikes per bin. At higher values of $g_{K(Ca)}$ our network responds with narrower bursts; that of Traub *et.al* with increased burst amplitude and lowered frequency. Most likely the difference stems from a difference between hippocampal pyramidal cells which are bursting and neocortical pyramidal cells where a majority is regular spiking. The difference may be explained as follows: Increased $g_{K(Ca)}$ leads to a larger (burst) synchronization (fig. 6a, and Traub *et al.* (1992) fig. 4 (our estimate), and (Ekeberg 1993)). In our simulations the burst amplitude does not increase despite of the synchronization, but is unchanged or decreased due to fewer spikes per burst as a result of the larger adaptation. A larger $g_{K(Ca)}$ is balanced by less calcium (fewer spikes) whereby the burst frequency remains constant. In the hippocampal pyramidal cell model the synchronization of the EPSP:s in the dendrites leads to a stronger Ca activation. The Ca-dependent depolarizing afterpotential (DAP) gives a burst of spikes producing a larger population burst amplitude (and more Ca). Increased Ca and $g_{K(Ca)}$ both give decreased burst frequency.

4 Discussion

The main contribution of this work is the demonstration that a network of mutually exciting neocortical pyramidal cells can produce sustained after-activity at rates close to those seen in cortex *in vivo*. This is a consequence of introducing saturating synapses in the network, which also improves biological realism. Here we investigate an extreme case of full saturation from one single spike, possibly in cortex 2–3 spikes may be necessary for full saturation. In addition, our study has also demonstrated that a simple network of neocortical pyramidal cells can display several different modes of operation. Below we will further discuss the context and significance of these findings.

4.1 The case for attractor models of cortical associative memory

As described in the introduction, the background of this work is attractor models of cortical associative memory functions, originating in Hebb's cell assembly theory, and mathematically implemented as Hopfield type ANNs. Such models have many merits but they have also been

criticized on several points. One of the main points of criticism has been that the feed-back excitation which is at their core, is bound to drive the participating cells to their maximum activity. For cortical pyramidal cells this would imply sustained firing rates up to 200–300 Hz. This is in sharp contrast to what is seen in cortical pyramidal cells *in vivo* where firing rates above some 60 s^{-1} are getting exponentially rare.

A number of ways of limiting firing rates in recurrent network models have been investigated, some of which use feed-back inhibition as a regulatory factor. We have presented an alternative biologically acceptable mechanism for obtaining low spike rates. The model is based on saturating synapses, the existence of which is well established experimentally (Andersen 1986), although the abundance of such synapses is uncertain. An additional effect of saturating synapses is that a specific set of input connections can only give limited excitation to the receiving cell allows it to remain in its dynamic range. This gives the cell a capability to sum over many input sources without saturating in its frequency response.

In a previous simulation study (Lansner and Fransén 1992) we showed that the processing time of a recurrent attractor network with pyramidal cells and inhibitory interneurons is in the order of 100 ms, which is compatible with what is seen in psychophysical reaction time experiments (Thorpe and Imbert 1989). Some recent results also show that introducing saturating synapses into the full network moves its operation towards low spiking rates without affecting significantly its pattern processing capabilities (Fransén and Lansner 1994; Lansner and Fransén 1994). Data from Abeles *et al.* (1990) is compatible with the hypothesis that the elementary units of cortical processing are distributed cell assemblies that each engage a small percentage of the whole population of cells. If neurons in an active cell assembly are assumed to have a firing rate of 50 s^{-1}, the probability to find such activity is 6 % over the time period for 6 % of the cells in the entire population. In addition low rate after-activity similar to that we consider here might also play a role in cortical processing related to working memory processes (Miyashita 1988; Miyashita and Chang 1988; Fuster and Jervey 1982; Funahashi *et al.* 1989, 1990).

The fact that robust low rate attractor activity is also possible in a network comprised of

realistic cells, as demonstrated here, improves further the case for recurrent attractor networks as models of cortical associative memory function.

4.2 Modulation of network dynamics

The simple network simulated here was capable of producing at least two qualitatively different modes of operation, *i.e.* burst synchronization and oscillating tonic firing. It is important to note that all oscillatory activity in this network appears in the absence of synaptic inhibition.

In earlier studies we have also investigated the effect of neuromodulators that modify the conductance of Ca-dependent K-channels in the full attractor network model with several overlapping memories stored. It was shown that the pattern processing operation of such a network may be affected dramatically, *i.e.* responses are typically vigorous at high modulator levels and weak or absent at low. This general picture fits well with the presence of several diffuse monoamine projections of subcortical origin that have been implicated in *e.g.* the regulation of overall activity levels and attention.

If occurring in the cortex, the kinds of oscillations demonstrated here would be likely to show up in cortical field potentials. Such oscillations in the 10 Hz range (6–20 Hz) have been observed in the post-stimulus time histogram (PSTH) of cells in several neocortical areas using different protocols (Dinse *et al.* 1990). Oscillations in this frequency range are also implicated by numerous experimental studies and models of *e.g.* the olfactory cortex (Hasselmo *et al.* 1992; Bressler and Freeman 1980; Freeman 1979).

To further assess the biological relevance of our network and cell model, we have compared the dynamics of our system with that of the disinhibited hippocampal slice. This is the biological system closest to our current network that has been studied experimentally and by means of simulations (Traub *et al.* 1992). Taking into consideration that the assembly also should be isolated from the other assemblies, this is not an entirely comparable situation, but it is the best one can do since locating and isolating a spatially distributed assembly experimentally would not be possible. As the experiments are done on a slice preparation, activity spreading is at least partially constrained. The modes of operation, when varying the conductances of the Ca-dependent K

channels and the strength of recurrent excitatory synapses in the models, were compared. The two systems behaved in a similar fashion. The differences observed may be explained by the differences in cellular properties reflected in the hippocampal and neocortical pyramidal cell models: Hippocampal CA3 pyramidal cells are intrinsically bursting which is rare for neocortical cells. The hippocampal cell has active dendrites, whereas except for synaptic ion channels the dendrites of our model neocortical pyramidal cell are purely passive. Ion channels that may provide for active properties of dendrites most likely exist in neocortical pyramidal cells as well, although their source and distribution remain unclear (Adams 1992). We have used a combined kainate/AMPA and NMDA synapse and Traub *et.al* used a non-NMDA AMPA synapse. Changing our synapse to a pure kainate/AMPA synapse enabled our network to burst also at the higher frequencies they report and gave even more similar burst shapes.

4.3 The role of cortical inhibition

Our simulation results clearly show that a simple network without inhibitory interneurons can by itself produce low-rate activity and oscillations of a kind seen in real cortex. This opens up for the interpretation that cortical inhibition may not be as critically involved in regulating firing rates of individual cells and producing oscillatory activity, as has often previously been assumed. From the perspective of the cell assembly theory, the role for inhibition in preventing spread of activity among overlapping assemblies and in the shaping of cellular response properties could be emphasized. In fact, in the neocortex a reduction of the inhibition by only 30 % (Lindström 1994) leads to epileptiform seizures. This may be interpreted as an example of activity spreading uncontrollably when inhibition no longer separates the partly overlapping assemblies.

5 Conclusions

We have shown that low firing rates can be obtained in an attractor network of mutually exciting pyramidal cells using a biologically fairly detailed cell model with saturating synaptic conductances. The network can produce low rate after-activity when a neuromodulator is applied. This demonstrates that recurrent attractor network models of cortical associative memory can operate

at the relatively low firing rates observed in cortical cells. Further, our simulations demonstrate clearly that a relatively simple network without inhibitory neurons can express complex oscillatory dynamics in some respects matching that seen in the real cortex.

6 Acknowledgments

We are grateful to Lennart Brodin, Örjan Ekeberg, Hans Liljenström, Staffan Johansson and Sivert Lindström for valuable discussions and comments on the manuscript, and to Örjan Ekeberg and Per Hammarlund for providing and improving the simulation software. This work was supported by the Swedish Natural Science Research Council, grant no F–FU 06445–307.

References

Abeles M, Vaadia E, Bergman H (1990) Firing patterns of single units in the prefrontal cortex and neural network models. Network **1**:13–25.

Adams P R (1992) The platonic neuron gets the hots. Current Biol. **2**:625–627.

Amit D J, Evans M R, Abeles M (1990) Attractor neural networks with biological probe records. Network **1**:381–405.

Amit D J, Treves A (1989) Associative memory neural network with low temporal spiking rates. Proc. Natl. Acad. Sci. USA **86**:7871–7875.

Amit D J, Tsodyks M V (1991a) Quantitative study of attractor neural network retrieving at low spike rates: I. substrate–spikes, rates and neuronal gain. Network **2**:259–273.

Amit D J, Tsodyks M V (1991b) Quantitative study of attractor neural network retrieving at low spike rates: II. low-rate retrieval in symmetric networks. Network **2**:275–294.

Andersen P (1986) Factors influencing the efficiency of dendritic synapses on hippocampal pyramidal cells. Neurosci. Res. **3**:521–530.

Andersen P (1990) Synaptic integration in hippocampal CA1 pyramids. Prog. Brain Res. **83**:215–222.

Bernander Ö, Douglas R J, Koch C (1992) A model of regular-firing cortical pyramidal neurons. Tech. Rep. CNS Memo 16, Computation and Neural Systems Program, California Institute of Technology, Pasadena CA, USA.

Bernander Ö, Douglas R J, Martin K A C, Koch C (1991) Synaptic background activity influences spatiotemporal integration in single pyramidal cells. Proc. Nat. Acad. Sci. USA **88**:11569–11573.

Bressler S L, Freeman W J (1980) Frequency analysis of olfactory system EEG in cat, rabbit and rat. Electroenceph. clin. Neurophysiol. **50**:19–24.

Brodin L, Tråvén H, Lansner A, Wallén P, Ekeberg Ö, Grillner S (1991) Computer simulations of N-methyl-D-aspartate (NMDA) receptor induced membrane properties in a neuron model. J. Neurophysiol. **66**:473–484.

Buhmann J (1989) Oscillations and low firing rates in associative memory neural networks. Phys. Rev. A **40**:4145.

Colino A, Halliwell J V (1987) Differential modulation of three separate K-conductances in hippocampal CA1 neurons by serotonin. Nature **328**:73–77.

Connors B W, Gutnick M J, Prince D A (1982) Electrophysiological properties of neocortical neurons in vitro. J. Neurophysiol. **48**:1302–1320.

Destexhe A, Mainen Z F, Sejnowski T J (1994) An efficient method for computing synaptic conductances based on a kinetic model of receptor binding. Neural Comp. **6**:14–18.

Dinse H R, Krüger K, Best J (1990) A temporal structure of cortical information processing. Concepts in Neuroscience **1**:199–238.

Douglas R J, Martin K A C (1991) A functional microcircuit for cat visual cortex. J. Physiol. **440**:735–769.

Ekeberg Ö (1993) Response properties of a population of neurons. Int. J. Neural Systems **4**:1–13.

Ekeberg Ö, Hammarlund P, Levin B, Lansner A (1994) SWIM — A simulation environment for realistic neural network modeling. In: Skrzypek J, ed. Neural Network Simulation Environments. Kluwer Hingham, MA.

Ekeberg Ö, Wallén P, Lansner A, Tråvén H, Brodin L, Grillner S (1991) A computer based model for realistic simulations of neural networks. I: The single neuron and synaptic interaction. Biol. Cybern. **65**:81–90.

Fransén E, Lansner A (1994) Low spiking rates in a network with overlapping assemblies. In: Bower J M, ed. The Neurobiology of Computation: Proceedings of the Annual Computational Neuroscience Meeting. Kluwer Boston, MA. (in press).

Fransén E, Lansner A, Liljenström H (1993) A model of cortical associative memory based on Hebbian cell assemblies. In: Eeckman F H, Bower J M, eds. Computation and Neural Systems. Kluwer Boston, MA, pp. 431–435.

Freeman W J (1979) EEG analysis gives model of neuronal template-matching mechanism for sensory search with olfactory bulb. Biol. Cybern. **35**: 221–234.

Funahashi S, Bruce C J, Goldman-Rakic P S (1989) Mnemonic coding of visual space in the monkey's dorsolateral prefrontal cortex. J. Neurophysiol. **61**: 331–349.

Funahashi S, Bruce C J, Goldman-Rakic P S (1990) Visuospatial coding in primate prefrontal neurons revealed by oculomotor paradigms. J. Neurophysiol. **63**: 814–831.

Fuster J M, Jervey J P (1982) Neuronal firing in the inferotemporal cortex of the monkey in a visual memory task. J. Neurosci. **2**: 361–375.

Gilbert C D, Hirsch J A, Wiesel T N (1990) Lateral interactions in visual cortex. In: Cold Spring Harbor Symposia on Quantitative Biology, volume LV. Cold Spring Harbor Laboratory Press. pp. 663–676.

Gustafsson B, Wigström H (1981) Evidence for two types of afterhyperpolarization in CA1 pyramidal cells in the hippocampus. Brain Res. **206**: 462–468.

Guthrie P B, Segal M, Kater S B (1991) Independent regulation of calcium revealed by imaging dendritic spines. Nature **354**: 76–79.

Hasselmo M E, Anderson B P, Bower J M (1992) Cholinergic modulation of cortical associative memory function. J. Neurophysiol. **67**: 1230–1246.

Hebb D O (1949) The Organization of Behavior. John Wiley New York.

Hestrin S, Nicoll R A, Perkel D J, Sah P (1990) Analysis of excitatory synaptic action in pyramidal cells using whole-cell recording from rat hippocampal slices. J. Physiol. **422**: 203–225.

Hopfield J (1982) Neural networks and physical systems with emergent collective computational abilities. Proc. Natl. Acad. Sci. USA **79**:2554–2558.

Koch C, Douglas R, Wehmeier U (1990) Visibility of synaptically induced conductance changes: Theory and simulations of anatomically characterized cortical pyramidal cells. J. Neurosci. **10**:1728–1744.

Lansner A, Fransén E (1992) Modelling Hebbian cell assemblies comprised of cortical neurons. Network **3**:105–119.

Lansner A, Fransén E (1994) Improving the realism of attractor models by using cortical columns as functional units. In: Bower J M, ed. The Neurobiology of Computation: Proceedings of the Annual Computational Neuroscience Meeting. Kluwer Boston, MA. (in press).

Liljenström H, Hasselmo M (1993) Acetylcholine and cortical oscillatory dynamics. In: Eeckman F H, Bower J M, eds. Computation and Neural Systems. Kluwer Boston, MA, pp. 523–530.

Lindström S (1994). (personal communication).

Madison D V, Nicoll R A (1982) Noradrenaline blocks accomodation of pyramidal cell discharge in the hippocampus. Nature **299**:636–638.

Mason A, Larkman A (1990) Correlations between morphology and electrophysiology of pyramidal neurons in slices of rat visual cortex. II. electrophysiology. J. Neurosci. **10**:1415–1428.

McCormick D A (1989) Cholinergic and noradrenergic modulation of thalamocortical processing. TINS **12**:215–221.

McCormick D A, Connors B W, Lighthall J W (1985) Comparative electrophysiology of pyramidal and sparsely spiny stellate neurons of the neocortex. J. Neurophysiol. **54**:782–806.

Milner P M (1957) The cell assembly: Mark II. Psychol. Rev. **64**:242–252.

Miyashita Y (1988) Neuronal correlate of visual associative long-term memory in the primate temporal cortex. Nature **335**:817–820.

Miyashita Y, Chang H S (1988) Neuronal correlate of pictorial short-term memory in the primate temporal cortex. Nature **331**:68–70.

Müller W, Connor J A (1991) Dendritic spines as individual neuronal compartments for synaptic Ca^{2+} responses. Nature **354**:73–76.

Nakamura K, Mikami A, Kubota K (1991) Unique oscillatory activity related to visual processing in the temporal pole of monkeys. Neurosci. Res. **12**:293–299.

Nicoll R A, Malenka R C, Kauer J A (1990) Functional comparison of neurotransmitter receptor subtypes in mammalian central nervous system. Physiol. Rev. **70**:513–565.

Ogawa T, Ito S, Kato H (1981) Membrane characteristics of visual cortical neurons in in vitro slices. Brain Res. **226**:315–319.

Peretto P (1992) An Introduction to the Modeling of Neural Networks. Cambridge University Press Cambridge.

Rubin N, Sompolinsky H (1989) Neural networks with low local firing rates. Europhys. Lett. **10**:465–470.

Scholfield C N (1978) Electrical properties of neurons in the olfactory cortex in vitro. J. Physiol. **275**:535–546.

Shepherd G M, Koch C (1990) Dendritic electrotonus and synaptic integration. In: Shepherd G M, ed. The Synaptic Organization of the Brain. Oxford University Press New York and Oxford. pp. 462.

Stafstrom C E, Schwindt P C, Crill W E (1984) Repetetive firing in layer V neurons from cat neocortex in vitro. J. Neurophysiol. **52**:264–277.

Stern P, Edwards F A, Sakmann B (1992) Fast and slow components of unitary EPSCs on stellate cells elicited by focal stimulation in slices of rat visual cortex. J. Physiol. **449**:247–278.

Thorpe S, Imbert M (1989) Biological constraints on connectionist modelling. In: Pfeifer R, ed. Connectionism in Perspective. Springer Verlag Berlin.

Traub R D, Miles R, Buzsáki G (1992) Computer simulation of carbachol-driven rhythmic population oscillations in the CA3 region of the *in vitro* rat hippocampus. J. Physiol. **451**:653–672.

Traub R D, Wong R K S, Miles R, Michelson H (1990) A model of a CA3 hippocampal pyramidal neuron incorporating voltage-clamp data on intrinsic conductanses. J. Neurophysiol. **66**:635–650.

Tråvén H, Brodin L, Lansner A, Ekeberg Ö, Wallén P, Grillner S (1993) Computer simulations of NMDA and non-NMDA receptor-mediated synaptic drive — sensory and supraspinal modulation of neurons and small networks. J. Neurophysiol. **70**:695–709.

Vogt B A (1985) Electrophysiological properties of cingulate neurons. In: Peters A, Jones E G, eds. Cerebral Cortex 4. Plenum Press New York and London. pp. 133–149.

Wallén P, Ekeberg Ö, Lansner A, Brodin L, Tråvén H, Grillner S (1992) A computer-based model for realistic simulations of neural networks. II: The segmental network generating locomotor rhythmicity in the lamprey. J. Neurophysiol. **68**: 1939–1950.

Fig 1. Lower trace: Soma membrane potential of the pyramidal cell RS. Stimulation with 0.5 nA for 120 ms. Upper trace: The RS-cell with modulator factor KCa of 0.5 applied. Stimulation with 0.5 nA for 120 ms.

Fig 2. Spike firing adaptation curves for the RS-cell without modulator and with a modulator factor KCa of 0.5. The inverse interspike interval is plotted against the spike interval number. Currents (nA) and presence of modulator (*) as indicated in legend.

Fig 3. Postsynaptic cell membrane potential for a cell driven at 22 Hz (lower part) and 227 Hz (upper part). The different synapses are a summing (S) or a saturating (T) kainate synapse or an NMDA synapse (N). Conductances are the same as described in sect 2.1.

Fig 4. Relation between input and output frequency for a postsynaptic cell driven with noisy synapses (Poisson distributed activity). The postsynaptic cell is driven by 10 synapses, each of which has the average frequency indicated on the abscissa. The absolute level of the frequency curves depends on the synaptic type and magnitude of the conductance. All types were tuned to give a starting point of 30 Hz (30 Hz is not the minimum firing frequency of a cell which is around 2 Hz). This resulted in a conductance for the summing kainate/AMPA synapse of 9.1 nS and 9.8 nS for the saturating one. For the NMDA synapse the conductance was 4.6 nS and for the combined type the kainate component was 4.3 nS and the NMDA was 2.6 nS. The large values are due to the small number of active synapses. The stable frequency point in a recurrent network is the (upper) intersection with the line $f_{out} = f_{in}$. sum = summing kainate component, sat = saturating kainate component, kA = pure kainate/AMPA synapse, NMDA = pure NMDA synapse, kA+N combined kainate and NMDA synapse.

Fig 5a. Bursting and after-activity. Mean spike rate plot of a network of 50 cells. Modulator factor (KCa) 0.6–1.0 and current stimulation (stim) 0.0–0.02 nA[3] as indicated. A driving current produces a train of bursts or, when a modulator is applied, continuous firing. When the modulator is applied low rate after-activity is seen when the driving current is terminated. In a network without synapses the cells fire at a rate of some 3 s^{-1}.

Fig 5b. Spike plot of fig 5a. In each row the occurrence of a spike in the corresponding cell is indicated.

Fig 6a. After-activity as a function of amount of modulator. Mean spike rate plot. Current stimulation 0.02 nA^3 for 50 ms and modulator factor KCa as indicated in legend.

Fig 6b. Mean spike rate plot showing rate of after-activity. The mean rate (mean) is plotted for the "standard" case with saturating synapses and modulator factor KCa 0.6. The distribution of the rates had a standard deviation of 21 Hz. As a control, mean rate for summing synapses, of smallest possible conductance (lowest rate) and with modulator factor KCa 0 (sum 0.0) or 1 (sum 1.0), are also shown. These curves have a high rate as was predicted in fig. 4. Current stimulation with 0.02 nA^3 for 50 ms.

Fig 7. Comparison to results of Traub *et.al* . A. Histograms for different synaptic conductances, values are fractions of our normal value. The modulator factor is 0.2. B. Histograms for different $g_{K(Ca)}$ values (the modulator factor value). The conductance fraction value is 0.6. Abscissas: simulation time 1 s, ordinates: 100 spikes per 10 ms bin.

[3]The current in fig. 5 and 6 is small compared to the currents displayed in fig. 2 because of the excitatory background stimulation (noise) that is added.

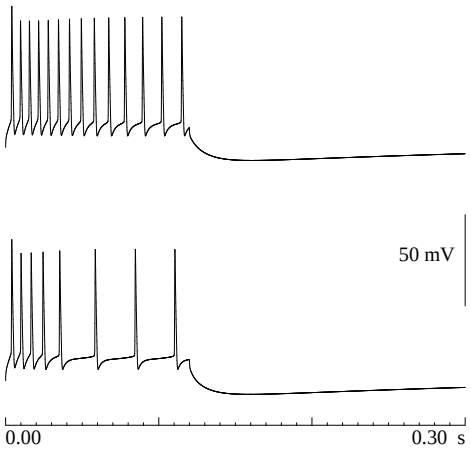

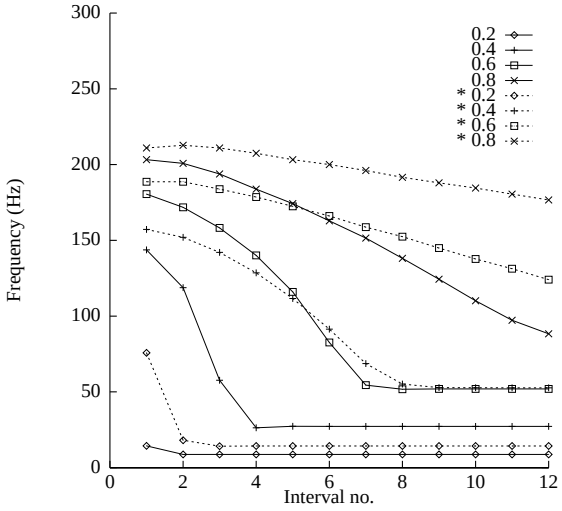

Fig 1. and 2.

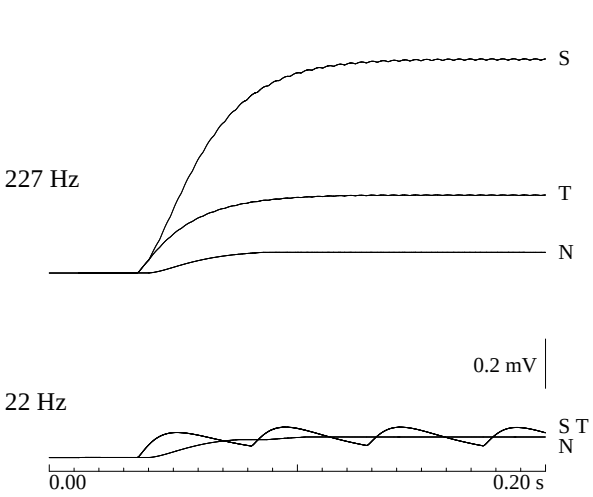

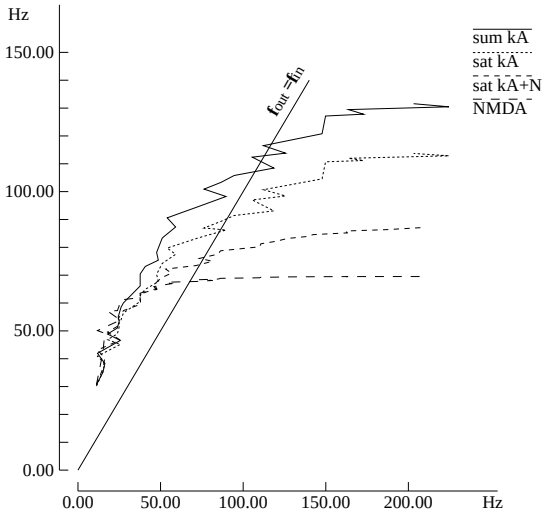

Fig 3. and 4.

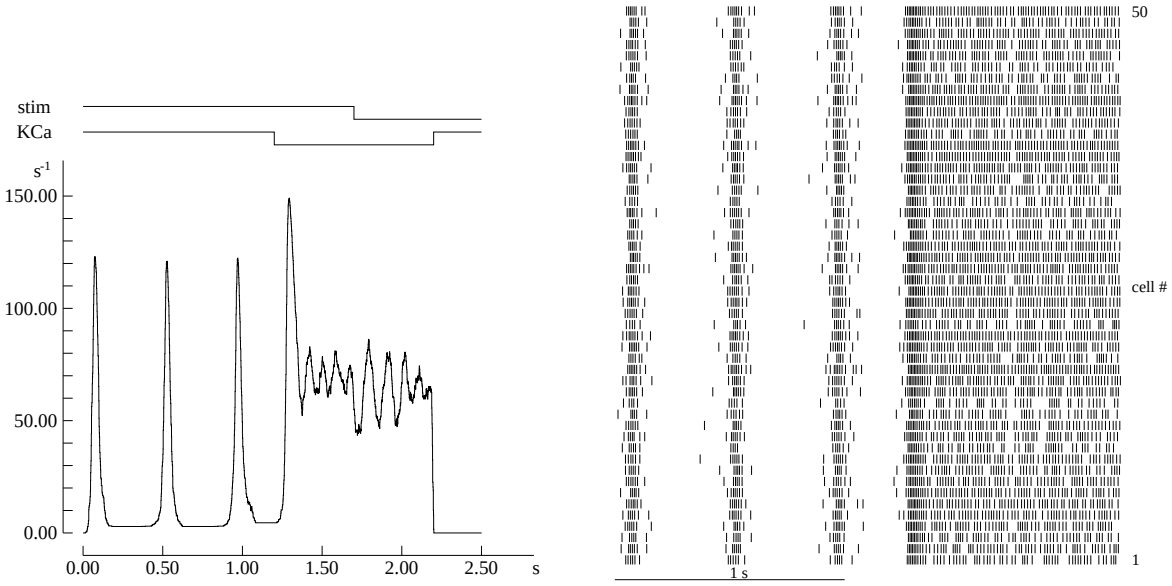

Fig 5a. and 5b.

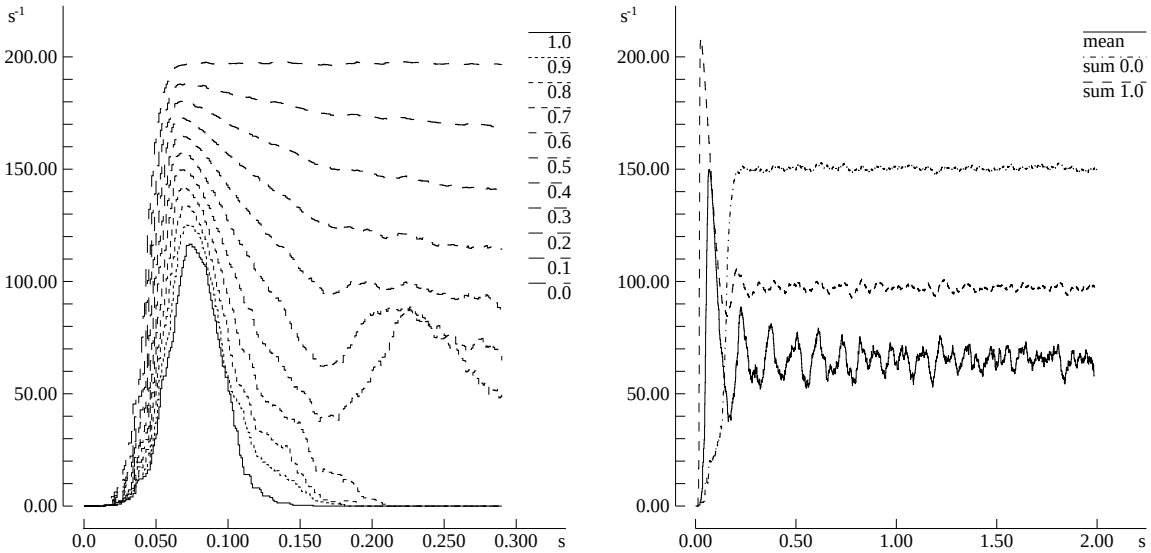

Fig 6a. and 6b.

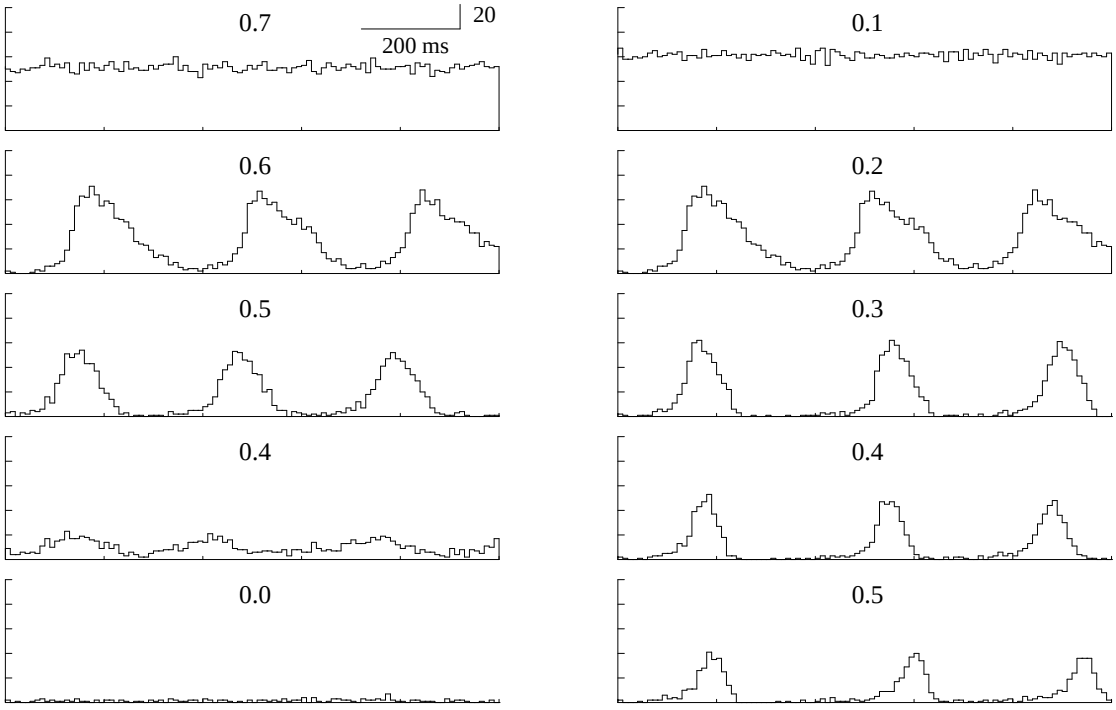

Fig 7a. and 7b.

Appendix

		Na^+		K^+	Ca^{2+}	NMDA
		m	h	n	q	p
α	A ($\mathrm{mV^{-1}\,ms^{-1}}$)	0.58	0.232	0.058	0.232	2.03 ($\mathrm{ms^{-1}}$)
	B (mV)	-50	-50	-50	10	–
	C (mV)	1	1	0.8	11	17
β	A ($\mathrm{mV^{-1}\,ms^{-1}}$)	0.174	1.16 ($\mathrm{ms^{-1}}$)	0.0145	0.0029	0.0292 ($\mathrm{ms^{-1}}$)
	B (mV)	-59	-46	-40	10	–
	C (mV)	20	2	0.4	0.5	17

Table 1 Parameters describing the ion channel kinetics.

Notes to table 1
Notations correspond to those used in Ekeberg *et al.* (1991). All parameters are according to Brodin *et al.* (1991) with the addition that the A-parameters in the Hodgkin-Huxley equations have been increased by a factor 2.9 to compensate for the higher temperatures (20–38 °C) used in *e.g.* McCormick *et al.* (1985), Stern *et al.* (1992) and Ogawa *et al.* (1981) compared to that used by Wallén *et al.* (1992) and Tråvén *et al.* (1993) (7–9 °C). The B-parameters have also been shifted -5 mV to give a threshold potential of -50 mV (Scholfield 1978; Connors *et al.* 1982) and (McCormick *et al.* 1985; Stern *et al.* 1992). [4]

*Parameter**	*Value†*	*Note*	*Unit*	*Description*
E_{leak}	-75	a	mV	leak current equilibrium potential
E_{Na}	50		mV	sodium current equilibrium potential
E_K	-80		mV	potassium current equilibrium potential
E_{Ca}	150		mV	calcium current equilibrium potential (voltage gated)
$E_{Ca(NMDA)}$	20		mV	calcium current equilibrium potential (NMDA gated)
g_m	0.44	b	$\mu S mm^{-2}$	membrane leak conductance
C_m	0.01		$\mu F mm^{-2}$	membrane capacitance
g_{ext}	0.0681	c	$nS mm^{-2}$	conductance from diffuse transmitter stimulation
Soma				parameters specific for the soma compartment
g_{Na}	150	d	$\mu S mm^{-2}$	sodium conductance
g_K	84		$\mu S mm^{-2}$	potassium conductance
$g_{K(Ca)}(AHP)$	36.8×M	e	$\mu S mm^{-2}$	potassium conductance (Ca^{2+} gated)
ρ_{AP}	1.0	e	$mV^{-1}\,ms^{-1}\,mm^{-2}$	Ca^{2+} inflow rate (voltage gated)
δ_{AP}	9	e	s^{-1}	Ca^{2+} decay rate (voltage entered Ca^{2+})
a_s	0.00139	f	mm^2	soma membrane mean area
Initial segment				parameters specific for the initial segment
g_{Na}	2505		$\mu S mm^{-2}$	sodium conductance
g_K	418		$\mu S mm^{-2}$	potassium conductance
g_{core}	300		$\mu S mm^{-2}$	core conductance per membrane area
a_{IS}	0.1		-	initial segment membrane area factor (fraction of soma area)
Dendrite				parameters specific for the dendrite compartments
g_{core}	8.1	g	$\mu S mm^{-2}$	core conductance per membrane area
a_d	4	h	-	dendrite membrane area factor (fraction of soma area)

Table 2 Parameters describing the cell.
Here, M is the modulator multiplication factor. *Notations correspond to those used in Ekeberg *et al.* (1991). †Values are the same as in Wallén *et al.* (1992) unless followed by a reference.

Notes to table 2
[a] E_{leak} is chosen to give the cell an (*in vitro*) soma membrane resting potential as described in McCormick *et al.* (1985), Scholfield (1978) and Connors *et al.* (1982).
[b] g_m is calculated from the time constant reported in McCormick *et al.* (1985), Scholfield (1978) and Bernander *et al.* (1991).
[c] g_{ext} is adjusted to give an (*in vivo*) resting potential of -65 mV, see also the discussions in Scholfield (1978), Connors *et al.* (1982), Bernander *et al.* (1991) and Vogt (1985) on *in vitro* and *in vivo* potentials.
[d] g_{Na} has been adjusted to give a larger spike height and shorter spike rise time (McCormick *et al.* 1985).
[e] ρ_{AP}, δ_{AP}, and $g_{K(Ca)}$(AHP) have been tuned to fit experimental curves (McCormick *et al.* 1985; Connors *et al.* 1982; Stern *et al.* 1992; Bernander *et al.* 1992; Mason and Larkman 1990; Stafstrom *et al.* 1984), see sect 2.2 for a discussion.
[f] a_s soma area from McCormick *et al.* (1985). Similar values are found in Bernander *et al.* (1992) and Douglas and

[4] our estimate

Martin (1991). [5]
[g] g_{core} is calculated from length constants in Hestrin *et al.* (1990) and Koch *et al.* (1990), see also the discussion in Shepherd and Koch (1990) p 462 on the ever shorter electrotonic lengths used in simulations.
[h] a_d dendritic tree area similar to that used in Bernander *et al.* (1992), and within the range used in Douglas and Martin (1991). [6]

*Parameter**	*Value†*	*Note*	*Unit*	*Description*
kainate/AMPA synapse				parameters specific for the kainate/AMPA synapse
compartment	*medial*	j	-	location
E_{Na+K}	0		mV	equilibrium potential for Na^+/K^+ current
g_{exc}	80	m	pS	conductance after spike
t_{delay}	1		ms	time delay
$t_{duration}$	0		ms	open time
ρ_{syn}	0		ms	raise time constant
δ_{syn}	10		ms	closing (decay) time constant
NMDA synapse				parameters specific for the NMDA synapse
compartment	*medial*	k	-	location
E_{NMDA}	0		mV	equilibrium potential for Na^+/K^+ current
$E_{Ca(NMDA)}$	20		mV	equilibrium potential for Ca^{2+} current
g_{NMDA}	560	m	pS	conductance after spike
t_{delay}	5		ms	time delay
$t_{duration}$	20		ms	open time
ρ_{syn}	5		ms	raise time constant
δ_{syn}	150		ms	closing (decay) time constant
noise synapse				parameters specific for the noise synapse
compartment	*proximal*		-	location
E_{noise}	0		mV	equilibrium potential for noise synapse
g_{noise}	105	n	$pSmm^{-2}$	conductance of noise synapse
δ_{syn}	10		ms	closing (decay) time constant

Table 3 Parameters describing the synapse.
*Notations correspond to those used in Tråvén *et al.* (1993). †Values are the same as in Tråvén *et al.* (1993) unless followed by a reference.

Notes to table 3
[j,k] The synaptic connection between RS-cells is a combined kainate/AMPA and NMDA synapse with equal amplitude contributions to the EPSP. It has been placed on the medial dendritic compartment.
[m] The standard deviation of the conductance of each synaptic type is 20 % of its mean value.
[n] g_{noise}: The conductance of the noise is tuned to give some 1–3 spikes per 10 s. As described in Wallén *et al.* (1992) the source of the synaptic noise is a Poisson process with an expectation value of 300 PSP:s per second.

[5] our estimate
[6] our estimate